Ion permeation and block of the gating pore in the voltage sensor of $Na_V1.4$ channels with hypokalemic periodic paralysis mutations

Stanislav Sokolov, Todd Scheuer, and William A. Catterall

Department of Pharmacology, University of Washington, Seattle, WA 98195

Hypokalemic periodic paralysis and normokalemic periodic paralysis are caused by mutations of the gating charge–carrying arginine residues in skeletal muscle $Na_V1.4$ channels, which induce gating pore current through the mutant voltage sensor domains. Inward sodium currents through the gating pore of mutant R666G are only ~1% of central pore current, but substitution of guanidine for sodium in the extracellular solution increases their size by 13- ± 2-fold. Ethylguanidine is permeant through the R666G gating pore at physiological membrane potentials but blocks the gating pore at hyperpolarized potentials. Guanidine is also highly permeant through the proton-selective gating pore formed by the mutant R666H. Gating pore current conducted by the R666G mutant is blocked by divalent cations such as Ba^{2+} and Zn^{2+} in a voltage-dependent manner. The affinity for voltage-dependent block of gating pore current by Ba^{2+} and Zn^{2+} is increased at more negative holding potentials. The apparent dissociation constant (K_d) values for Zn^{2+} block for test pulses to −160 mV are 650 ± 150 µM, 360 ± 70 µM, and 95.6 ± 11 µM at holding potentials of 0 mV, −80 mV, and −120 mV, respectively. Gating pore current is blocked by trivalent cations, but in a nearly voltage-independent manner, with an apparent K_d for Gd^{3+} of 238 ± 14 µM at −80 mV. To test whether these periodic paralyses might be treated by blocking gating pore current, we screened several aromatic and aliphatic guanidine derivatives and found that 1-(2,4-xylyl)guanidinium can block gating pore current in the millimolar concentration range without affecting normal $Na_V1.4$ channel function. Together, our results demonstrate unique permeability of guanidine through $Na_V1.4$ gating pores, define voltage-dependent and voltage-independent block by divalent and trivalent cations, respectively, and provide initial support for the concept that guanidine-based gating pore blockers could be therapeutically useful.

INTRODUCTION

Voltage-gated sodium channels in skeletal muscle ($Na_V1.4$) respond to nerve stimulation by generating action potentials that initiate excitation–contraction coupling. They are composed of a large, pore-forming α subunit of 1,840 amino acid residues and a β1 subunit of 218 amino acid residues (Barchi, 1983; Trimmer et al., 1989; Isom et al., 1992; Catterall, 2000). The α subunit is organized in four homologous domains containing six transmembrane segments each (S1–S6). The S4 transmembrane segments in each domain contain the primary gating charges—typically four or more arginine or lysine residues spaced at three-residue intervals (Bezanilla, 2000; Catterall, 2000). The S5 and S6 transmembrane segments and the P loop between them form the pore, and the short intracellular loop connecting domains III and IV serves as the fast-inactivation gate (Bezanilla, 2000; Catterall, 2000). The gating charges in the voltage sensors of sodium channels and other voltage-gated ion channels respond to membrane depolarization by moving outward across the transmembrane electric field (Hodgkin and Huxley, 1952), which causes charge movement that can be measured directly as a capacitative current preceding channel activation (Armstrong, 1981). Approximately 12 gating charges move outward upon activation of voltage-gated sodium channels (Hirschberg et al., 1995; Bezanilla, 2000).

Mutations in skeletal muscle sodium channels cause multiple forms of dominantly inherited periodic paralysis (Cannon, 2006; Venance et al., 2006). Paramyotonia congenita and hyperkalemic periodic paralysis are caused by mutations that are widespread in the sodium channel protein and either enhance activation or impair inactivation of sodium channels, leading to dominant gain of sodium channel function and hyperexcitability (Cannon, 2006). In contrast, mutations that cause hypokalemic periodic paralysis (HypoPP) and normokalemic periodic paralysis neutralize one of the gating charges in an S4 segment of $Na_V1.4$ channels or the corresponding amino acid residues in skeletal muscle calcium channels ($Ca_V1.1$; Venance et al., 2006), but conventional physiological studies of these mutations have not revealed consistent functional effects that might cause these diseases (Jurkat-Rott et al., 2000; Struyk et al., 2000; Bendahhou et al., 2001; Kuzmenkin et al., 2002). The convergence

Correspondence to William A. Catterall: wcatt@u.washington.edu

Abbreviations used in this paper: HypoPP, hypokalemic periodic paralysis; TTX, tetrodotoxin.

The Rockefeller University Press $30.00
J. Gen. Physiol. Vol. 136 No. 2 225–236
www.jgp.org/cgi/doi/10.1085/jgp.201010414

of these mutations on the gating charges of the voltage sensors in both the skeletal muscle sodium channel and skeletal muscle calcium channel strongly implicates alterations in voltage sensor function in this disease.

The function of the voltage sensors of ion channels is to transduce changes in membrane potential into a conformational change that opens the pore. This is achieved by movement of positive gating charges in S4 transmembrane segments across the membrane under the influence of the electric field (Bezanilla, 2000; Catterall, 2000). According to the sliding helix model of gating, the gating charges in S4 segments are thought to move through a specialized pathway or "gating pore" formed by the S1, S2, and S3 segments of voltage-sensing domains (Catterall, 1986; Guy and Seetharamulu, 1986; Yang et al., 1996; Gandhi and Isacoff, 2002). Conserved negative charges in these segments are proposed to form sequential ion–pair interactions with the positive gating charges of S4 as they traverse the transmembrane electric field (Catterall, 1986; Papazian et al., 1995; Yarov-Yarovoy et al., 2006; DeCaen et al., 2008). Consistent with this mechanism, mutations of the arginine gating charges in sodium or potassium channels to smaller, uncharged residues render the voltage sensors permeable to protons and/or cations, giving rise to gating pore currents through the modified voltage sensor (Starace and Bezanilla, 2004; Sokolov et al., 2005; Tombola et al., 2005). Mutations of outer gating charges in $Na_V1.4$ channels cause gating pore current in the resting state, whereas mutations of inward gating charges cause gating pore current in the activated state (Sokolov et al., 2005). This voltage dependence is expected if the gating pore is blocked by the arginine gating charges as they traverse the membrane.

Naturally occurring mutations in $Na_V1.4$ channels that cause HypoPP and normokalemic periodic paralysis induce gating pore currents resulting from ionic leak through the mutant voltage sensors (Sokolov et al., 2007, 2008; Struyk and Cannon, 2007; Struyk et al., 2008). In the present study, we investigated the biophysical properties of the mutant gating pore in domain II of HypoPP mutant $Na_V1.4$ channels in more detail. We found that gating pores in $Na_V1.4$ HypoPP mutants R666G and R666H in domain II conduct guanidinium ion much better than Na^+. We determined that the mutant voltage sensors in slow-inactivated R666G channels can conduct gating pore current even better than in the resting state, and we confirmed that Na^+ currents through the gating pore can be blocked by Ba^{2+} and Zn^{2+}. Our results show that block by divalent cations is voltage dependent at negative holding potentials. In contrast, trivalent cations such as Gd^{3+}, La^{3+}, and Yb^{3+} can block Na^+ gating pore currents with IC_{50} values in the range of 200–300 µM, but the block is voltage independent. Among several organic guanidine derivatives tested, 1-(2,4-xylyl)guanidine is capable of blocking gating pore current in the millimolar concentration range without alteration of sodium channel function. Substituted guanidines with higher affinity may have promise as therapeutic agents in the treatment of HypoPP.

MATERIALS AND METHODS

Materials

Restriction endonucleases and other molecular biology reagents were purchased from New England Biolabs, Inc. and Roche. pCDM8 vector and the MC1061 *Escherichia coli* bacterial strain were purchased from Life Technologies. cDNA encoding rat $Na_V1.4$ α subunit (Trimmer et al., 1989; Featherstone et al., 1998) subcloned into pCDM8 (Yu et al., 2003) was used as a template for site-directed mutagenesis and expression in *Xenopus laevis* oocytes. Mutations R666G and R666H were described previously (Sokolov et al., 2007).

Expression in *Xenopus* oocytes

pCDM8 plasmids encoding wild-type and mutant $Na_V1.4$ α subunits were linearized with HpaI, and plasmids encoding β1 subunits were linearized with HindIII. Transcription was performed with T7 RNA polymerase (Applied Biosystems). Isolation, preparation, and maintenance of *Xenopus* oocytes were performed as described previously (McPhee et al., 1995). Healthy stage V–VI oocytes selected manually were pressure injected with 50 nl of solution containing varying ratios of α- and β1-subunit RNA. Electrophysiological recordings were performed 5–10 d after injection.

Cut-open oocyte voltage clamp

Cut-open oocyte voltage clamp experiments were performed as previously described (Sokolov et al., 2007, 2008). Capacity transients were partially compensated with the voltage clamp amplifier circuitry at a holding potential used in a particular experiment (CA-1; Dagan Corporation). 1 µM tetrodotoxin (TTX) was present in all solutions to block central pore conductance. Oocytes were preconditioned in TTX-containing solutions for at least 10 min before recording. Cells were held for at least 5 min at any given holding potential before gating pore current measurements. All gating pore current measurements were performed without leak subtraction. Gating pore current amplitudes were measured by averaging the last 0.5 ms of 50-ms test pulses. Voltage-independent nonspecific leak was subtracted offline by fitting current-voltage relationships in the range between 0 and 40 mV with a linear function and subtracting the resulting linear leak current. Gating charge movement was determined in every cell as a measure of expression level for normalization using the protocol depicted in Fig. 2 A and −P/10 leak subtraction from a holding potential of 0 mV. Cells with <0.7 nC of total gating charge were excluded from calculations of normalized values.

The intracellular solution consisted of 110 mM K-methanesulfonate, 10 mM Na-methanesulfonate, 10 mM EGTA, and 10 mM HEPES, pH 7.4. The extracellular solution (1.8Ca solution) contained 1.8 mM Ca-methanesulfonate and 10 mM HEPES, pH 7.4, in addition to primary charge carrier: 120 mM Na-methanesulfonate, 120 mM *N*-methyl-D-glucamine methanesulfonate, or combinations of these cations with guanidine sulfate or ethylguanidine sulfate as described in figure legends.

The starting volume of the upper recording chamber (CC1-D; Dagan Corporation) was 150 µl. For experiments involving the addition of divalent or trivalent cations, guanidine, or guanidine derivatives, 2× concentrated stocks of corresponding solutions in 1.8Ca solution were freshly prepared and used within 3 h after dilution. 2× stocks were added to the recording chamber to yield appropriate final concentrations. Recordings were

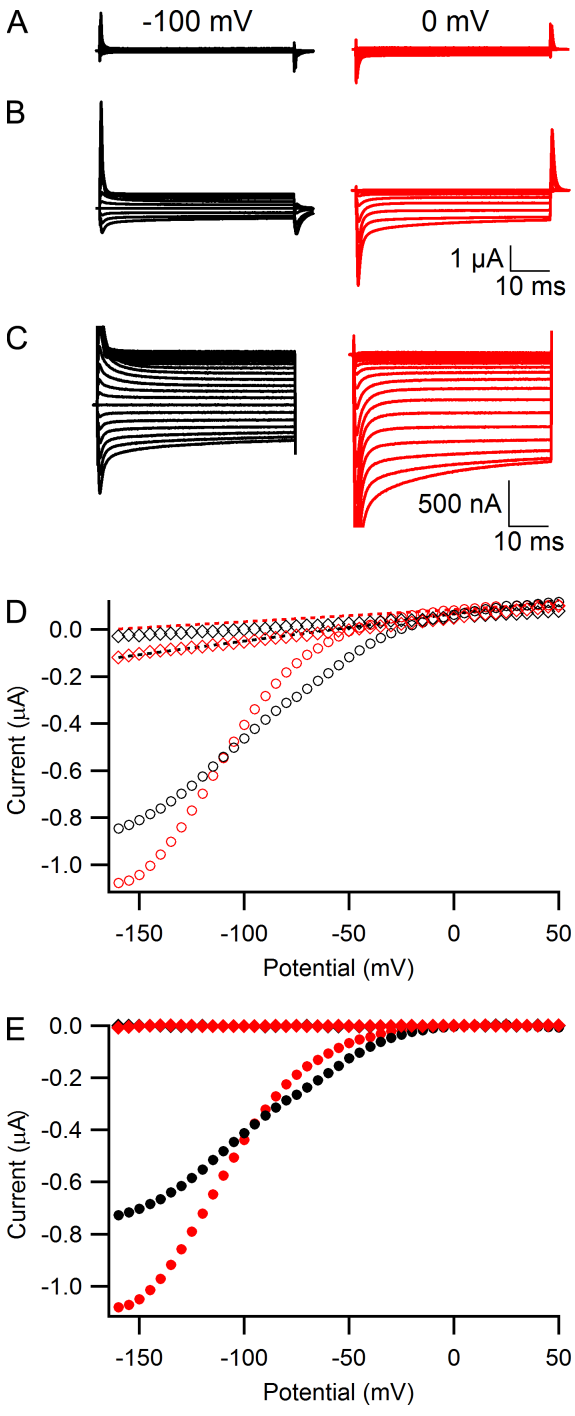

Figure 1. Gating pore currents in R666G at depolarized and hyperpolarized holding potentials. Currents were recorded in the presence of 1 μM TTX in response to a series of 50-ms voltage steps ranging from −160 mV to 50 mV in 5-mV increments from a holding potential of −100 mV (left panels and black symbols) or 0 mV (right panels and red symbols) without any leak subtraction. The external solution contained 120 mM NaOH, 1.8 mM $Ca(OH)_2$, and 10 mM HEPES, pH 7.4, with methanesulfonic acid. Currents through the wild-type $Na_V1.4$ (A) and R666G (B) channels are shown on a scale where both gating charge displacement and gating pore currents can be observed and compared. Every fourth trace is shown for clarity. (C) Records from B are shown on an expanded scale, focusing on gating pore currents. Every second trace is shown for clarity. (D) Voltage dependence of representative currents in A and B before leak subtraction (open symbols): diamonds, $Na_V1.4$ wild type; circles, R666G. Dotted lines are linear fits to the data in the voltage range between 0 and 40 mV used for offline subtraction of linear leak through cell membrane. (E) Voltage dependence of leak-subtracted gating pore currents (closed symbols): diamonds, $Na_V1.4$ wild type; circles, R666G.

performed 2 min after addition to ensure proper diffusion. The following salts were used for preparation of solutions: $BaCl_2$, Na_2EDTA, $ZnSO_4$, $ZnCl_2$, $GdCl_3$, $YbCl_3$, $LaCl_3$, $LuCl_3$, YCl_3, $TlCl_3$, $HfCl_4$, guanidine sulfate, guanidine carbonate, and 1-(2,4-xylyl) guanidine carbonate. Adjustment of pH was performed by titration with methanesulfonic acid to pH 7.4. For experiments in Fig. 4 C, the external solutions were present in the recording chamber from the beginning of the oocyte mounting procedure. All experiments were performed at room temperature.

Microelectrodes were pulled from borosilicate glass capillary tubes (1.5-mm OD; A-M Systems) and had resistances of 250–350 kΩ when filled with 3 M KCl. Currents were filtered at 5 kHz with a low-pass Bessel filter and digitized at 20 kHz. Voltage commands were generated using Pulse 8.5 software (HEKA) and an ITC-18 analogue to digital interface (Instrutech). Data were analyzed with Igor Pro (WaveMetrics). Voltage clamp protocols are described in the figure legends. Pooled data are reported as means ± SEM. Statistical comparisons were performed using Student's *t* test, with $P < 0.05$ as the criterion for significance.

RESULTS

Gating pore currents in the resting and slow-inactivated states

The $Na_V1.4$ HypoPP mutant R666G (rat $Na_V1.4$; equivalent to R672G in humans) conducts inward cation currents at negative membrane potentials through the gating pore in the mutant voltage sensor (Sokolov et al., 2007). We analyzed the properties of R666G gating pore by expressing the $Na_V1.4$/R666G α subunit and the β1 subunit in *Xenopus* oocytes and measuring ionic currents using the cut-open voltage clamp technique (Stefani and Bezanilla, 1998; Sokolov et al., 2007) in the presence of 1 μM TTX to block the central pore. As we reported previously (Sokolov et al., 2007), when the extracellular medium contains 120 mM Na^+ and 1.8 mM Ca^{2+} but no other divalent cations (1.8Ca solution), total leak currents through membranes of oocytes expressing wild-type $Na_V1.4$ channel (Fig. 1 A) were small and linear with holding potentials of −100 mV or 0 mV (Fig. 1, A and D, open diamonds). In oocytes expressing the R666G mutant, a series of 50-ms test pulses applied in 5-mV steps revealed inward ionic currents with nonlinear voltage dependence at negative test potentials (Fig. 1, B–D, open circles). These gating pore currents were substantially smaller than capacitative transients (Fig. 1 B), but they were typically 5–10-fold larger than the nonspecific linear leak through the cell membrane (Fig. 1 D, dotted lines) and thus can be well resolved. Gating pore

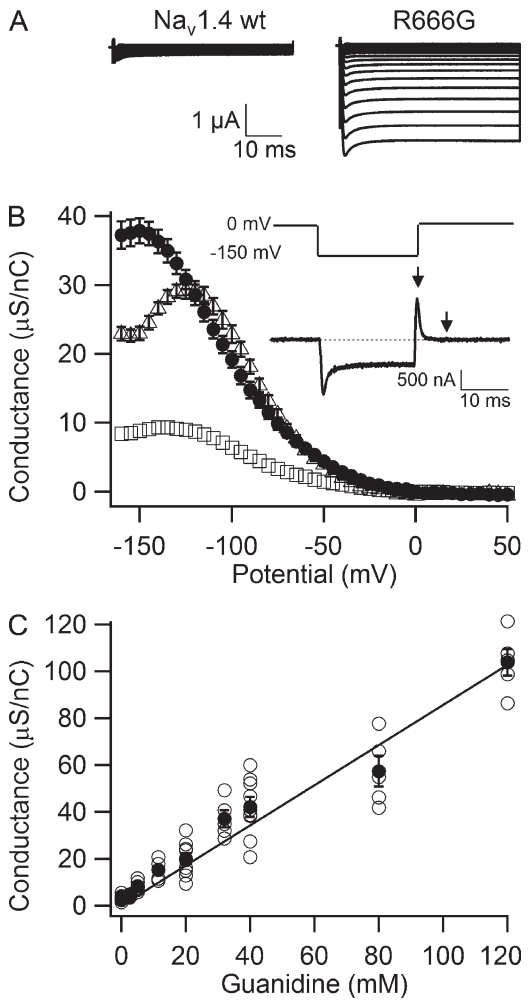

Figure 2. Permeability of guanidinium ion through the R666G gating pore. (A) Representative gating pore currents through the wild-type $Na_V1.4$ and R666G channels in an external solution containing 80 mM NMDG + 40 mM guanidinium as permeant cations. (B) Conductance-voltage relationship of gating pore conductance for 120 mM Na^+ (open squares, $n = 20$), 40 mM guanidinium (closed circles, $n = 7$), and 40 mM ethylguanidinium (open triangles, $n = 5$). (inset) Voltage protocol and representative record of gating charge movement used for normalization of gating pore currents to gating charge. −P/10 subtraction from a holding potential of 0 mV was used to subtract capacity transients. A 20-ms voltage step to −150 mV was followed by repolarization to 0 mV. Gating charge was calculated by integrating the current transient evoked by this repolarization step (area between the arrows). (C) Dependence of normalized guanidinium conductance on concentration. Currents were first recorded in 120 mM NMDG solution and then after addition of increasing concentrations of guanidinium (open circles, individual experiments; closed circles, mean, $n \geq 5$). Error bars represent SEM.

currents obtained after maintaining the cell membrane for 5 min at 0 mV (Fig. 1 C, red) were substantially larger than gating pore currents measured at a holding potential of −100 mV (Fig. 1 C, black). At depolarized holding potentials, wild-type $Na_V1.4$ channels enter the slow-inactivated state, where they do not conduct central pore currents (Kuzmenkin et al., 2002). Interestingly, gating pore currents in R666G are 30–40% larger in the slow-inactivated state at a holding potential of 0 mV (Fig. 1 E, red symbols) than in the resting state at a holding potential of −100 mV (Fig. 1 E, black symbols). Because holding the oocyte membrane at 0 mV, at which gating pore current is not active, makes them more stable in prolonged experiments, we used 0 mV as a holding potential throughout this study except where indicated otherwise.

Guanidinium permeation through the R666G gating pore

The gating pores of mutant *Shaker* K^+ channels and mutant Na_V channels conduct multiple monovalent cations nonselectively (Sokolov et al., 2005, 2007; Tombola et al., 2005, 2007). The guanidinium ion, which mimics the guanidinium group of the native arginine side chain, is about twofold more permeable through the *Shaker* R1C gating pore than K^+ (Tombola et al., 2005). In contrast, guanidinium is dramatically more permeant than Na^+ for the R666G mutant (Fig. 2). In the presence of 40 mM guanidinium, we observed much larger gating pore currents than in 120 mM Na^+ (compare Fig. 2 A with Fig. 1 B). In fact, guanidinium gating pore currents are so large they obscure capacitative transients. These guanidinium currents are specific for the R666G mutant voltage sensor and are not observed in wild-type $Na_V1.4$ (Fig. 2 A, left).

To normalize gating pore currents to expression level in individual cells, we used measurements of gating charge movement in response to a change in transmembrane voltage. Because the gating charge that moves across the membrane upon depolarization or repolarization is proportional to the number of R666G channels with active voltage sensors in the membrane, this quantification provides an estimate of relative channel density on the cell surface. The traditional method of measuring gating charge movement, which involves depolarization from a negative holding potential and use of negative leak-subtraction pulses, is compromised in the R666G channel by the presence of the large gating pore current at these potentials. Therefore, we used an alternative method depicted in the inset of Fig. 2 B. In this protocol, we used a holding potential of 0 mV and −P/10 leak subtraction from 0 mV to subtract residual capacity transients and the linear component of leak current. This holding potential was chosen because the mutant gating pore is not actively conducting at 0 mV. A 20-ms hyperpolarizing step to −150 mV restored >90% (not depicted) of the gating charge from immobilization by inactivation (Q_{off} current transient in Fig. 2 B, inset) and induced gating pore current (plateau in Fig. 2 B, inset). The voltage was then returned to a holding potential of 0 mV, creating a Q_{on} gating charge transient (Fig. 2 B, inset, arrow), which was relatively unaffected by gating pore current. We integrated this Q_{on} gating charge current (the area between arrows in Fig. 2 B, inset) and used this estimate

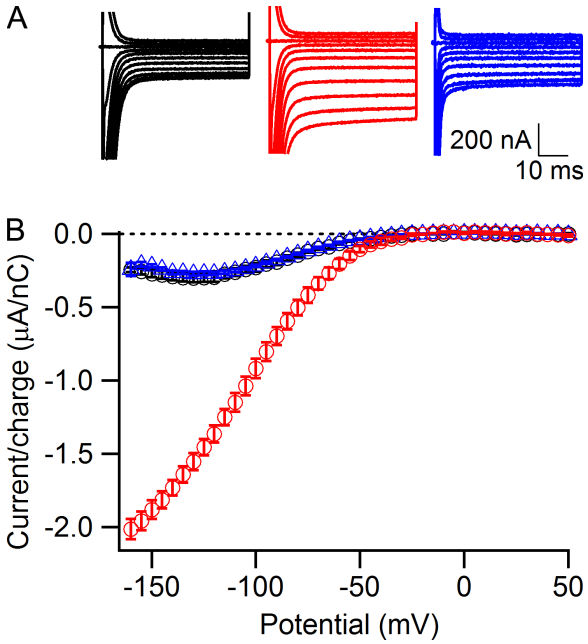

Figure 3. Permeability of guanidinium through the R666H gating pore. (A) Gating pore currents in representative oocytes expressing R666H channels recorded first in external solution containing 120 mM NMDG at pH 7.4 (left, black traces) and then in external solution containing 60 mM NMDG + 60 mM guanidinium at pH 7.4 (middle, red traces). Right panel (blue traces), gating pore current in a cell with a similar level of expression recorded in external solution containing 60 mM NMDG + 60 mM Na^+, pH 7.4. Test pulses were recorded in 5-mV increments and shown in 20-mV increments for clarity. (B) Averaged voltage dependence of leak-subtracted and normalized gating pore currents in solutions containing 120 mM NMDG (black circles, $n = 4$), 60 mM NMDG + 60 mM guanidinium (red circles, $n = 4$), and 60 mM NMDG + 60 mM Na^+ (blue triangles, $n = 8$). Error bars represent SEM.

of charge movement for normalization of sodium channel expression level throughout this study.

Normalized slope conductance was estimated by calculating the differential of the current-voltage relationship at each point in 5-mV steps as previously described (Sokolov et al., 2008) and was plotted against the test-pulse voltage for 120 mM Na^+ (Fig. 2 B, open squares), 40 mM guanidinium (Fig. 2 B, closed circles), and 40 mM ethylguanidinium (Fig. 2 B, open triangles). Ethylguanidinium is even closer in structure and size to the arginine side chain than guanidinium itself, yet Tombola et al. (2005) reported that 10 mM ethylguanidinium was impermeant through the mutant R1C *Shaker* channel gating pore and blocked about half of the K^+ gating pore conductance. For the R666G mutant of $Na_V1.4$ channels, the R2 side chain in the domain II voltage sensor is absent altogether, allowing ethylguanidinium to pass through this gating pore at rates comparable to the smaller guanidinium ion (Fig. 2 B, open triangles). Na^+ and guanidinium conductance-voltage curves have similar voltage dependence peaking at −130 to −140 mV and decreasing slightly at more negative potentials. In contrast, the ethylguanidinium curve peaks at a less negative potential, near −120 mV, and declines abruptly at more negative membrane potentials (Fig. 2 B, open triangles). These results indicate that ethylguanidinium can block the mutant gating pore at membrane potentials more negative than −120 mV. Guanidinium conductance in R666G is linearly dependent on concentration (Fig. 2 C) and is 13- ± 2-fold higher than Na^+ conductance.

Guanidinium permeation through the R666H gating pore

We have shown previously that the HypoPP mutant R666H is capable of conducting gating pore current at hyperpolarized membrane potentials (Sokolov et al., 2007), and Struyk and Cannon (2007) demonstrated that this arginine to histidine substitution produces a mutant gating pore that selectively conducts protons under physiological conditions. In accordance with these previous results, the gating pore current recorded in the presence of 60 mM Na^+ and 60 mM NMDG at pH 7.4 is not significantly different from gating pore current recorded in 120 mM NMDG at pH 7.4 (Fig. 3, black circles and blue triangles). However, we observed an approximately sevenfold increase in the amplitude of the gating pore current after addition of 60 mM guanidinium ion to the external solution (Fig. 3, red circles). Thus, even when the bulky histidine side chain replaces R666, the mutant gating pore is still highly permeable to guanidinium ions.

Voltage-dependent block of Na^+ gating pore currents in R666G by Ba^{2+}

In our previous study, we reported that the divalent cations Ca^{2+}, Ba^{2+}, and Zn^{2+} can block Na^+ currents through the R666G gating pore at millimolar concentrations (Sokolov et al., 2007), but block by divalent cations was not observed by Struyk et al. (2008). Here we confirm that Ba^{2+} inhibits gating pore currents carried by Na^+ and examine this phenomenon in more detail (Fig. 4). To evaluate Ba^{2+} block quantitatively at a fixed membrane potential, we compared amplitudes of gating pore currents recorded in either 1.8Ca external solution or in external solution containing 1.5 mM Ca^{2+} + 2.5 mM Ba^{2+}, the same divalent composition used in the experiments of Struyk and Cannon (2007) and Struyk et al. (2008). Gating pore currents were measured at the end of 50-ms test pulses to −160 mV after ≥5 min at a holding potential of 0 mV, leak subtracted, and normalized to gating charge as described in Fig. 2 B (Fig. 4, A and B). The data from individual cells were fitted with linear function with zero intercept for both 1.8Ca solution (Fig. 4 B, black circles) and a 1.5-mM Ca^{2+} + 2.5-mM Ba^{2+} solution (Fig. 4 B, red triangles). Comparing the slopes of these fits reveals that, when the holding potential is 0 mV, ∼40% of gating pore current during test pulses to −160 mV is blocked in the presence of 2.5 mM Ba^{2+}.

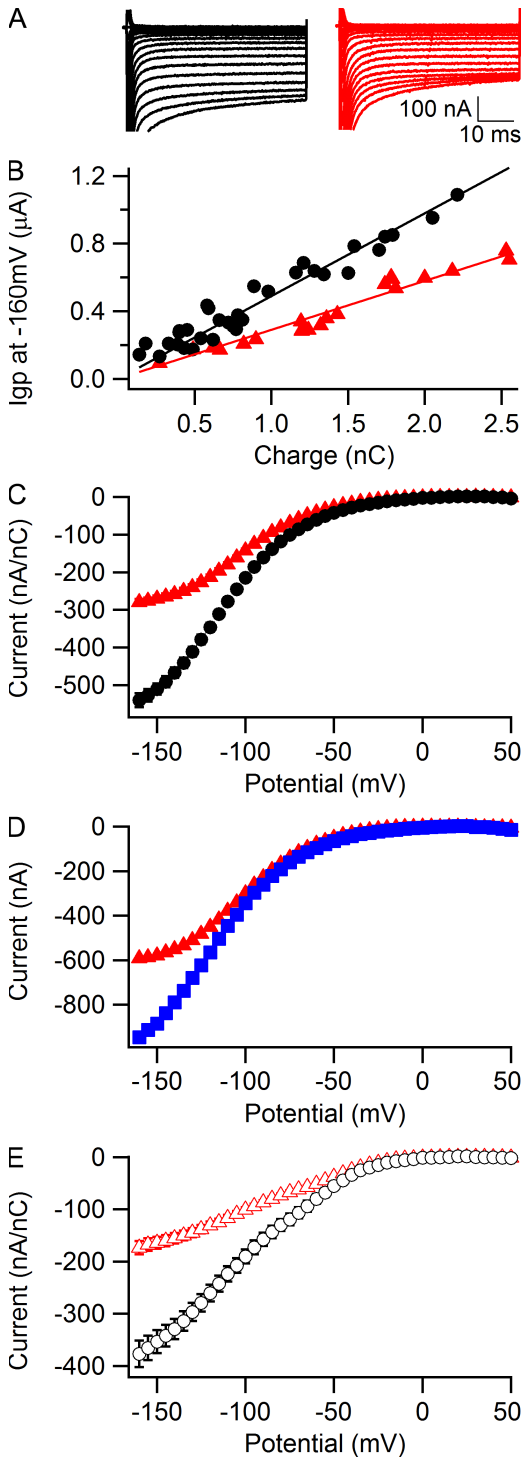

Figure 4. Block of Na^+ gating pore currents in R666G by Ba^{2+}. (A) Gating pore current in a representative cell recorded from a holding potential of 0 mV in external solution containing 120 mM Na^+ or 1.8 mM Ca^{2+} (black traces) and again after addition of 2.5 mM $BaCl_2$ (red traces). (B) Steady-state inhibition of gating pore currents by 2.5 mM Ba^{2+} assessed by plotting gating pore current amplitude versus gating charge for currents measured during a test pulse to −160 mV from a holding potential of 0 mV in either 1.8Ca solution (black circles) or a 1.5-mM Ca^{2+} + 2.5-mM Ba^{2+} solution (red triangles). Each symbol represents an individual oocyte. Data were fitted with linear function with zero intercept and slopes k_{Ca} = 490 ± 11 nA/nC and k_{Ba} = 290 ± 6 nA/nC. (C) Averaged current-voltage plots for gating currents measured from a holding potential of 0 mV in either 1.8-mM Ca^{2+} solution (black circles, n = 16) or a 1.5-mM Ca^{2+} + 2.5-mM Ba^{2+} solution (red triangles, n = 14). (D) Effect of chelation of Ba^{2+} with EDTA. Gating pore currents in a representative cell were first recorded in a 1.5-mM Ca^{2+} + 2.5-mM Ba^{2+} external solution (red triangles) and then after addition of 4 mM EDTA to external solution (blue squares). (E) Averaged current-voltage plots for gating currents measured from a holding potential of −100 mV in either a 1.8-mM Ca^{2+} solution (open black circles, n = 10) or 1.5-mM Ca^{2+} + 2.5-mM Ba^{2+} solution (open red triangles, n = 9).

The effect of 2.5 mM Ba^{2+} on the current-voltage relationship measured from a holding potential of 0 mV is illustrated in Fig. 4 C. A significant reduction of gating pore current is observed at test potentials more negative than −100 mV in the presence of Ba^{2+}, demonstrating a voltage-dependent block by this divalent cation. To further substantiate the voltage-dependent effects of Ba^{2+}, we performed experiments in which Ba^{2+} block was reversed by application of divalent cation chelator EDTA to the external solution (Fig. 4 D). Gating pore currents were first measured in a 1.5-mM Ca^{2+} + 2.5-mM Ba^{2+} solution (Fig. 4 D, red triangles) and again after addition of 4 mM EDTA (Fig. 4 D, blue squares). Chelation of free Ba^{2+} (together with free Ca^{2+}) by EDTA increases gating pore current, with most of its effect occurring at voltages negative to −100 mV. On average, 4 mM EDTA caused a 48 ± 8% increase of gating pore current measured at −160-mV test potential (n = 6). Together, these results demonstrate reversible, voltage-dependent block of gating pore current by Ba^{2+}.

Finally, we evaluated the effects of Ba^{2+} at a holding potential of −100 mV (Fig. 4 E), the same holding potential used in the studies by Struyk and Cannon (2007) and Struyk et al. (2008). As observed previously for 1.8Ca solution (Fig. 1 E), switching holding potential from 0 to −100 mV for 5 min produced a substantial reduction of gating pore current amplitudes (Fig. 4, compare E with C). In addition to this effect, the presence of 2.5 mM Ba^{2+} in external solution caused a further 54 ± 7% reduction of gating pore current measured during test pulses to −160 mV (Fig. 4 E, 1.8Ca solution, open black circles; 1.5-mM Ca^{2+} + 2.5-mM Ba^{2+} solution, open red triangles). These results directly demonstrate voltage-dependent block by Ba^{2+} at a holding potential of −100 mV.

Voltage-dependent block of Na^+ gating pore currents in R666G by Zn^{2+}

We reported previously that Zn^{2+} blocks gating pore current in R666G with substantially higher affinity than Ba^{2+} (Sokolov et al., 2007). Accordingly, when 2.5 mM Zn^{2+} is added to the external solution at a holding potential of −80 mV, it blocks ∼80% of the gating pore current (Fig. 5, A and B). A full concentration dependence curve for Zn^{2+} block of gating pore current recorded during test pulses to −160 mV (Fig. 5 B) yielded an IC_{50} value of

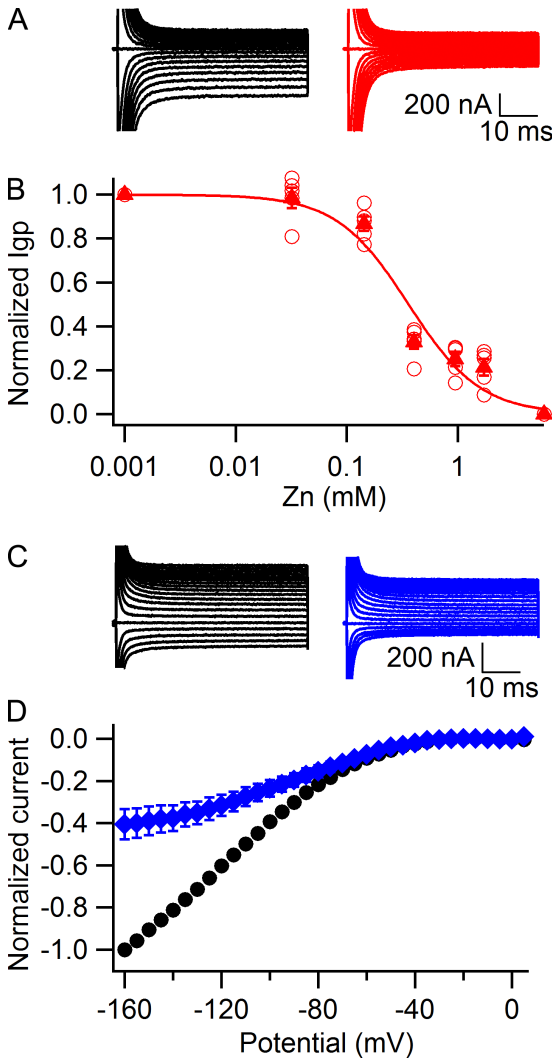

Figure 5. Block of Na^+ gating pore currents in R666G by Zn^{2+}. (A) Gating pore current in a representative cell recorded from a holding potential of −80 mV first in 120 mM Na^+, 1.8-mM Ca^{2+} external solution (left, black traces), and after addition of 2.5 mM $ZnSO_4$ (right, red traces). (B) Concentration dependence of gating pore current block by Zn^{2+} assessed at a −80-mV holding potential (open circles, individual experiments; closed triangles, mean, $n = 5$). The solid red line is a fit of the averaged data with the Hill equation: rate= 1.3 ± 0.3, IC_{50} = 0.36 ± 0.07 mM. (C) Representative gating pore currents recorded with a −120-mV holding potential in 120 mM Na^+, 1.8-mM Ca^{2+} external solution (left, black traces), and after addition of 143 µM $ZnSO_4$ (right, blue traces). (D) Normalized leak-subtracted current-voltage relationships for Na^+ gating pore currents recorded with a −120-mV holding potential in control 1.8Ca external solution (black circles, $n = 6$) and in the presence of 143 µM Zn^{2+} (blue diamonds, $n = 6$). Error bars represent SEM.

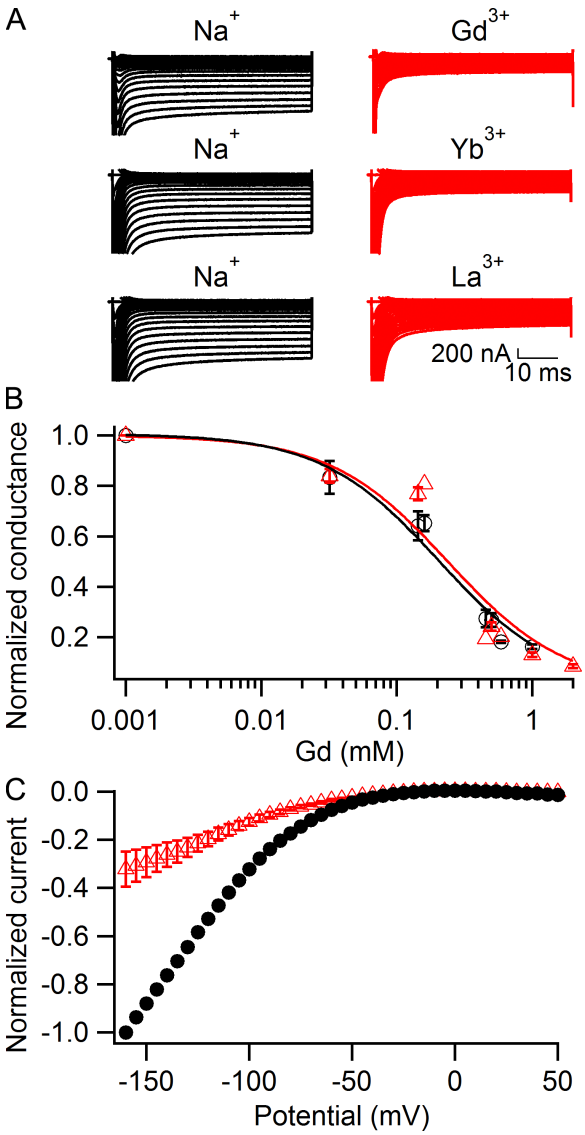

Figure 6. Block of Na^+ gating pore currents in R666G by trivalent cations Gd^{3+}, Yb^{3+}, and La^{3+}. (A) Representative gating pore currents recorded in 120 mM Na^+, 1.8-mM Ca^{2+} external solution (left, black traces), and after addition of 5 mM $GdCl_3$ (top right), 5 mM $YbCl_3$ (middle right), or 5 mM $LaCl_3$ (bottom right). (B) Concentration dependence of Gd^{3+} block at either 0-mV holding potential (black circles; IC_{50} = 207 ± 10 µM, $n = 4$–6) or −80-mV holding potential (red triangles; IC_{50} = 238 ± 14 µM, $n = 3$–6). (C) Normalized leak-subtracted current-voltage relationships for Na^+ gating pore currents recorded with a −80-mV holding potential in control 1.8Ca external solution (black circles, $n = 5$) and in the presence of 500 µM Gd^{3+} (red triangles, $n = 4$). Error bars represent SEM.

360 ± 70 µM at −80 mV. The apparent affinity for Zn^{2+} increased at a more negative holding potential of −120 mV, where 143 µM Zn^{2+} caused a 60 ± 7% reduction in gating pore current recorded at −160 mV (Fig. 5, C and D, blue). This concentration of Zn^{2+} caused only a 13 ± 3% reduction of the gating pore current when the holding potential was −80 mV (Fig. 5 B). These results are consistent with an apparent K_d value of 96 ± 11 µM for Zn^{2+} block when measured from a holding potential of −120 mV, compared with 360 ± 70 µM when measured from a holding potential of −80 mV (Fig. 5 B) and 650 ± 150 µM at a holding potential of 0 mV (not depicted). These results indicate that block of the R666G gating pore by Zn^{2+} is substantially increased at more negative holding potentials.

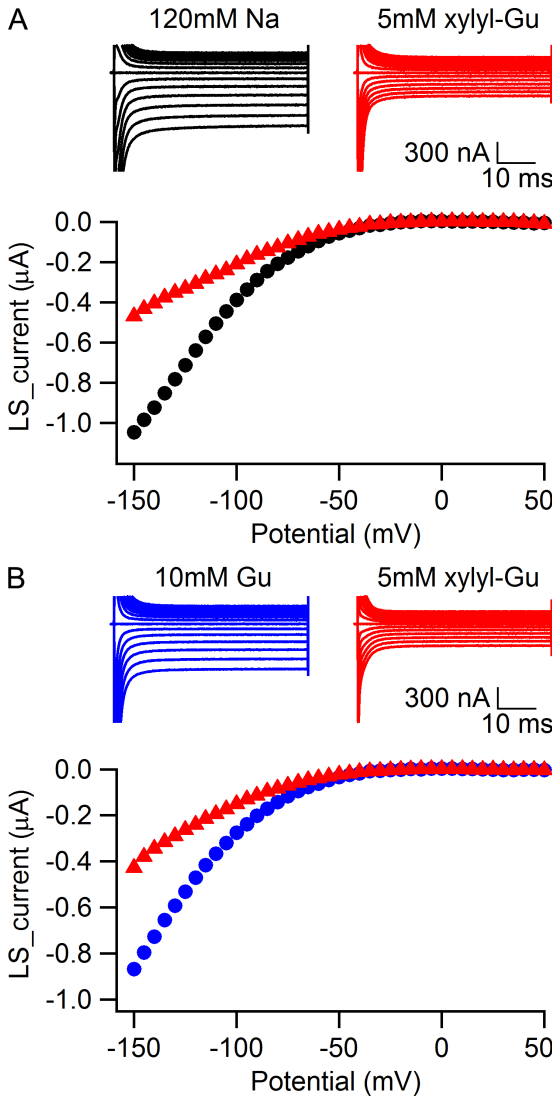

Figure 7. 1-(2,4-xylyl)guanidine blocks R666G gating pore currents. (A) Sodium gating pore current in a representative cell was first measured in 120 mM Na^+, 1.8-mM Ca^{2+} external solution (black traces), and after addition of 5 mM 1-(2,4-xylyl)guanidine carbonate to external solution (red traces). The holding potential was 0 mV. Leak-subtracted currents are plotted against the voltage in the bottom panel. (B) Guanidinium gating pore current in a representative cell first measured in solution containing 115 mM NMDG, 10 mM guanidine sulfate, 1.8 mM Ca^{2+} (blue traces), and after addition of 5 mM 1-(2,4-xylyl)guanidine carbonate to external solution (red traces). The holding potential was 0 mV. Leak-subtracted current-voltage relationships are plotted in the bottom panel.

Block of gating pore currents by trivalent cations

The trivalent cations Gd^{3+}, Yb^{3+}, and La^{3+} are potent blockers of some voltage-gated Ca^{2+} channels, store-operated Ca^{2+} channels, and transient receptor potential channels (Biagi and Enyeart, 1990; Lansman, 1990; Powis et al., 1994; Leffler et al., 2007) as well as Na^+ channels (Sheets and Hanck, 1992). We therefore examined the effects of these trivalent cations on gating pore currents in R666G (Fig. 6). We found that Gd^{3+}, Yb^{3+}, and La^{3+} (Fig. 6 A) as well as Lu^{3+}, Y^{3+}, Tl^{3+}, and Hf^{4+} (not depicted) all block gating pore current in a similar concentration range. We examined Gd^{3+} effects on gating pore currents in more detail (Fig. 6, B and C). The concentration dependence curves for Gd^{3+} block of I_{gp} obtained with holding potentials of 0 mV (Fig. 6, B and C, black circles) and −80 mV (Fig. 6, B and C, red triangles) were similar (IC_{50} = 207 ± 10 µM at a holding potential of 0 mV and 238 ± 14 µM at a holding potential of −80 mV), indicating that block of gating pore current by trivalent cations is independent of membrane potential. Consistent with voltage-independent block, when Gd^{3+} was applied at a holding potential of −80 mV (Fig. 6 C), it did not produce substantial "flattening" of the current-voltage curve at negative voltages that is characteristic for Ba^{2+} (Fig. 4 D, red triangles) and Zn^{2+} (Fig. 5 D, blue diamonds). These results show that gating pore block by trivalent cations is not voltage dependent, in contrast to block by divalent cations. Divalent and trivalent cations may bind at separate sites along the permeation pathway, such that only the divalent cation binding site is deep enough within the membrane electrical field to cause significant voltage dependence of binding.

Block of R666G gating pore currents by a guanidine derivative

Because the guanidine-containing side chain of arginine is normally present in the gating pore, we searched for guanidine derivatives that would enter the gating pore and block it. As ethylguanidine carried gating pore current and only blocked the gating pore at negative potentials (Fig. 2 B), we tested several larger aliphatic and aromatic guanidinium compounds. Nine substituted guanidine compounds of varying structure were inactive at 1 mM. However, we found that 1-(2,4-xylyl)guanidine carbonate blocks gating pore currents in the 1–5-mM range (Fig. 7). The effects of 5 mM 1-(2,4-xylyl)guanidine on gating pore current carried by 120 mM Na^+ (Fig. 7 A) or 10 mM guanidinium (Fig. 7 B) were comparable. In parallel experiments, we found that this concentration of 1-(2,4-xylyl)guanidine had no substantial effect on the function of $Na_V1.4$ channels (unpublished data). Thus, 1-(2,4-xylyl)guanidine provides proof of the concept that small organic molecules containing a guanidine moiety might be useful therapeutically to block gating pore currents in muscle fibers without substantial side effects on normal sodium channel function.

DISCUSSION

Conductance of the gating pore in R666G in the slow-inactivated state

Gating pore current in the R666G mutant is greater when the holding potential is 0 mV than when it is −100 mV (Fig. 1). These results indicate that R666G channels in

the slow-inactivated state at 0 mV are capable of conducting gating pore current, and the size of the current is increased ~30–40% with respect to gating pore currents in the resting state. These results suggest that the conformation of the gating pore is different in resting and slow-inactivated channels, creating a permeation pathway with different conductance. The voltage dependence of gating charge movement in voltage-gated ion channels is shifted negatively when holding potential is made more positive (Bezanilla, 2000). The voltage dependence of gating pore current through the mutant voltage sensor in R666G also exhibits this characteristic negative shift at a holding potential of 0 mV (Fig. 1 E). This shift is appreciated most easily by comparing the voltage at which gating pore current begins to increase. Similar negative shifts in voltage dependence in response to holding potential are well documented for gating charge movements in voltage sensors and are thought to result from voltage sensor immobilization or relaxation at depolarized membrane potentials (Bezanilla, 2000; Villalba-Galea et al., 2008). Evidently, these conformational changes in the voltage sensor of R666G channels result in both altered voltage dependence and conductance of the gating pore.

Guanidinium ion is a selective permeant of gating pores

Mutations that induce gating pore currents typically convert an arginine gating charge to an amino acid with a smaller, less positively charged side chain. In light of this, guanidinium would be considered a likely permeant ion, and previous experiments showed that guanidinium is about twofold more permeant than K^+ through the R1C gating pore in *Shaker* K^+ channels (Tombola et al., 2005). In contrast to these earlier experiments, our results presented here show that guanidine is dramatically more permeant through mutant gating pores in domain II of $Na_V1.4$ channels, ~13-fold more permeant than Na^+ for R666G, and much more permeant than Na^+ for R666H, whose Na^+ permeability is too small to accurately distinguish from proton permeability. These results suggest that permeant ions pass through the same molecular route as the side chain of the gating charge–carrying arginine residues. The large gating pore currents recorded in solutions in which guanidinium substitutes for Na^+ could be a valuable tool in studies of gating pores in native skeletal muscle cells and in other experimental contexts where the density of $Na_V1.4$ channels is much less than in our transfected *Xenopus* oocytes.

Relative amplitudes of gating pore currents and central pore currents

In our previous studies (Sokolov et al., 2005, 2007), we compared the amplitude of gating pore currents to central pore currents in favorably transfected *Xenopus* oocytes in which the gating pore currents were large enough to measure accurately and the central pore currents were still well controlled by the voltage clamp. We found that gating pore currents conducted by R666G were ~1.2% of central pore currents. This approach of comparing gating pore with central pore currents has the advantage that it depends on direct measurements of current amplitudes without any assumptions about the open probability at certain voltages or the single-channel conductances at specific saline compositions. In contrast, Struyk et al. (2008) calculated gating pore current per $Na_V1.4$ channel by normalizing it to the amplitude of the gating charge movement and then compared that value to the known single-channel current of $Na_V1.4$ channels. They estimated that the gating pore current was only 0.05% of peak central pore current (Struyk et al., 2008). These estimates seem far apart at first glance but actually are comparable when the differences in experimental conditions and calculations are considered. Struyk et al. (2008) used a holding potential of −100 mV, at which gating pore conductance is substantially smaller than at the 0-mV holding potential used in our studies (Figs. 1 E and 4 C; Sokolov et al., 2007). Moreover, the presence of 2.5 mM Ba^{2+} in external solution used by Struyk et al. (2008) further reduces gating pore current (Fig. 4, C and E). Together, these effects account for an approximately threefold reduction in normalized gating pore current amplitudes (Fig. 4, compare C, black circles, with E, red triangles). Also, Struyk et al. (2008) used the single-channel conductance for comparison to central pore current, but the $Na_V1.4$ channel has a P_o of ~0.2 at the peak of the current-voltage relationship (Lawrence et al., 1996), so its contribution to central pore current is only 20% of the single-channel conductance on average. Correcting for these differences adjusts the estimate of the relative gating pore current of Struyk et al. (2008) to ~0.8% of central pore current, similar to the estimate of 1.2% we previously reported (Sokolov et al., 2007).

Divalent cations block the R666G gating pore in a voltage-dependent manner

Divalent cations, including Ba^{2+} and Zn^{2+}, block gating pore current in a voltage-dependent manner. In solutions containing 1.8 mM Ca^{2+} as the only divalent cation, gating pore current increases monotonically with hyperpolarization up to −160 mV, the most negative test potential at which we could consistently record without damage to the cut-open oocyte (Fig. 4 C, black circles). These results show that there is negligible saturation of the Na^+ gating pore current at negative membrane potentials under these physiological concentrations. In contrast, in the presence of divalent cations Ba^{2+} (Fig. 4 C, red triangles) or Zn^{2+} (Fig. 5 D, blue diamonds) in the extracellular solution and with negative holding potentials of −100 mV or −120 mV, saturation of the gating pore current at negative test potentials becomes substantial (Figs. 4 E and 5 D). This effect can be relieved by application

of divalent cation chelator EDTA to external solution (Fig. 4 D, blue squares). Thus, the saturation at negative potentials described by Struyk et al. (2008) in terms of a barrier model actually reflected voltage-dependent block by Ba^{2+} in their standard extracellular solution, which was enhanced at negative holding potentials.

Voltage-dependent block was also pronounced with Zn^{2+} in the extracellular solution, with apparent K_d values of 650 ± 150 µM, 360 ± 70 µM, and 96 ± 11 µM when measured from holding potentials of 0 mV, −80 mV, or −120 mV, respectively. Surprisingly, Struyk et al. (2008) did not observe this potent and complete block of gating pore current by Zn^{2+}. One possible explanation for this discrepancy is that Struyk et al. (2008) reported use of $Zn(OH)_2$, which is nearly insoluble in water, to make their solutions, whereas we used $ZnSO_4$, which is much more soluble in aqueous solutions. In this case, it is possible that the concentrations of Zn^{2+} in the solutions of Struyk et al. (2008) were much less than intended. Moreover, block by Zn^{2+} would also be occluded by the weaker block by Ba^{2+} under control conditions because of the 2.5 mM Ba^{2+} in the standard extracellular solutions of Struyk et al. (2008), so these two effects may have worked together to obscure the block by Zn^{2+}.

Our results suggest that voltage-dependent block arises from two distinct mechanisms. First, the voltage dependence of divalent cation binding causes increased block at negative test pulse potentials, as observed in current-voltage relationship plots. This effect may represent divalent cation binding in the gating pore within the membrane electric field. Second, prolonged depolarizations cause voltage-dependent conformational changes within the voltage sensor of the *Ciona intestinalis* voltage-sensitive phosphatase (Villalba-Galea et al., 2008). In sodium channels, such slow conformational changes are accompanied by slow inactivation of the central pore and are revealed as a hysteresis in the voltage dependence of activation versus deactivation of gating pore current (Bezanilla, 2000; Sokolov et al., 2008). Such slow conformational changes in the voltage sensor may modify the affinity of the divalent cation binding site in the mutant gating pore, resulting in stronger binding of Ba^{2+} and Zn^{2+} to the resting conformation of the mutant voltage sensor at negative holding potentials, and may therefore produce stronger block of gating pore current at negative potentials as observed in our experiments with different holding potentials. These two distinct mechanisms through which negative membrane potentials enhance voltage-dependent block of the gating pore are interesting topics for further study.

Trivalent cations block the R666G gating pore in a voltage-independent manner

Trivalent cations exhibit complex effects on voltage-gated Na^+, Ca^{2+}, and K^+ channels. These effects come from a combination of voltage-dependent open channel block and surface charge screening effects (Armstrong and Cota, 1990, 1999; Biagi and Enyeart, 1990; Hanck and Sheets, 1992; Büsselberg et al., 1993). Surface charge screening is dependent on the phospholipid composition of the membrane and is facilitated by the presence of negatively charged head group lipids such as phosphatidylserine (Ermakov et al., 2010). We found that the trivalent cations Yb^{3+}, Gd^{3+}, and La^{3+} are blockers of gating pore current with EC_{50} values in the concentration range of 200–300 µM (EC_{50} = 238 µM for Gd^{3+}). Surprisingly, despite the increase in valence, block by trivalent cations did not show the pronounced voltage dependence observed for divalent cations Ba^{2+} and Zn^{2+}. These results imply different sites for binding and block by divalent and trivalent cations. If block is caused by cation binding in the gating pore, the divalent cations may be able to enter farther into the pore within the transmembrane electric field, whereas the trivalent cations bind to a more superficial site external to the membrane electric field.

Organic derivatives of guanidine can block the R666G gating pore

The high permeability of the guanidinium ion through mutant gating pores suggested that permeant ions move through the mutant gating pore via the same molecular pathway as the arginine side chains of the gating charge–carrying arginine residues and therefore that the mutant gating pore might be blocked by organic compounds with guanidine groups. To test this idea, we studied 10 compounds in which a guanidine group was attached to a larger aliphatic or aromatic moiety. Only one of these compounds, 1-(2,4-xylyl)guanidine, had measurable blocking activity at millimolar concentrations. These results suggest that there is considerable structural specificity for block of the gating pore by guanidine compounds and that a larger, high-throughput survey of such compounds might yield blockers with high affinity and specificity. Because 1-(2,4-xylyl)guanidine has no effect on sodium channel function at a concentration that blocked gating pore current, such compounds may be useful therapeutically in preventing or relieving attacks of weakness in patients with HypoPP.

The authors would like to dedicate this work to the late Elizabeth M. Sharp, who provided excellent technical assistance in this research and in our previous experiments on gating pore currents.

This work was supported by grants from the National Institutes of Health (R01 NS15751) and the Muscular Dystrophy Association to W. A. Catterall.

Submitted: 4 February 2010
Accepted: 6 July 2010

REFERENCES

Armstrong, C.M. 1981. Sodium channels and gating currents. *Physiol. Rev.* 61:644–683.

Armstrong, C.M., and G. Cota. 1990. Modification of sodium channel gating by lanthanum. Some effects that cannot be

explained by surface charge theory. *J. Gen. Physiol.* 96:1129–1140. doi:10.1085/jgp.96.6.1129

Armstrong, C.M., and G. Cota. 1999. Calcium block of Na^+ channels and its effect on closing rate. *Proc. Natl. Acad. Sci. USA.* 96:4154–4157. doi:10.1073/pnas.96.7.4154

Barchi, R.L. 1983. Protein components of the purified sodium channel from rat skeletal muscle sarcolemma. *J. Neurochem.* 40:1377–1385.

Bendahhou, S., T.R. Cummins, R.C. Griggs, Y.H. Fu, and L.J. Ptácek. 2001. Sodium channel inactivation defects are associated with acetazolamide-exacerbated hypokalemic periodic paralysis. *Ann. Neurol.* 50:417–420. doi:10.1002/ana.1144

Bezanilla, F. 2000. The voltage sensor in voltage-dependent ion channels. *Physiol. Rev.* 80:555–592.

Biagi, B.A., and J.J. Enyeart. 1990. Gadolinium blocks low- and high-threshold calcium currents in pituitary cells. *Am. J. Physiol.* 259:C515–C520.

Büsselberg, D., B. Platt, H.L. Haas, and D.O. Carpenter. 1993. Voltage gated calcium channel currents of rat dorsal root ganglion (DRG) cells are blocked by Al^{3+}. *Brain Res.* 622:163–168. doi:10.1016/0006-8993(93)90815-5

Cannon, S.C. 2006. Pathomechanisms in channelopathies of skeletal muscle and brain. *Annu. Rev. Neurosci.* 29:387–415. doi:10.1146/annurev.neuro.29.051605.112815

Catterall, W.A. 1986. Voltage-dependent gating of sodium channels: correlating structure and function. *Trends Neurosci.* 9:7–10. doi:10.1016/0166-2236(86)90004-4

Catterall, W.A. 2000. From ionic currents to molecular mechanisms: the structure and function of voltage-gated sodium channels. *Neuron.* 26:13–25. doi:10.1016/S0896-6273(00)81133-2

DeCaen, P.G., V. Yarov-Yarovoy, Y. Zhao, T. Scheuer, and W.A. Catterall. 2008. Disulfide locking a sodium channel voltage sensor reveals ion pair formation during activation. *Proc. Natl. Acad. Sci. USA.* 105:15142–15147. doi:10.1073/pnas.0806486105

Ermakov, Y.A., K. Kamaraju, K. Sengupta, and S. Sukharev. 2010. Gadolinium ions block mechanosensitive channels by altering the packing and lateral pressure of anionic lipids. *Biophys. J.* 98:1018–1027. doi:10.1016/j.bpj.2009.11.044

Featherstone, D.E., E. Fujimoto, and P.C. Ruben. 1998. A defect in skeletal muscle sodium channel deactivation exacerbates hyperexcitability in human paramyotonia congenita. *J. Physiol.* 506:627–638. doi:10.1111/j.1469-7793.1998.627bv.x

Gandhi, C.S., and E.Y. Isacoff. 2002. Molecular models of voltage sensing. *J. Gen. Physiol.* 120:455–463. doi:10.1085/jgp.20028678

Guy, H.R., and P. Seetharamulu. 1986. Molecular model of the action potential sodium channel. *Proc. Natl. Acad. Sci. USA.* 83:508–512. doi:10.1073/pnas.83.2.508

Hanck, D.A., and M.F. Sheets. 1992. Extracellular divalent and trivalent cation effects on sodium current kinetics in single canine cardiac Purkinje cells. *J. Physiol.* 454:267–298.

Hirschberg, B., A. Rovner, M. Lieberman, and J. Patlak. 1995. Transfer of twelve charges is needed to open skeletal muscle Na^+ channels. *J. Gen. Physiol.* 106:1053–1068. doi:10.1085/jgp.106.6.1053

Hodgkin, A.L., and A.F. Huxley. 1952. The dual effect of membrane potential on sodium conductance in the giant axon of Loligo. *J. Physiol.* 116:497–506.

Isom, L.L., K.S. De Jongh, D.E. Patton, B.F.X. Reber, J. Offord, H. Charbonneau, K. Walsh, A.L. Goldin, and W.A. Catterall. 1992. Primary structure and functional expression of the β1 subunit of the rat brain sodium channel. *Science.* 256:839–842. doi:10.1126/science.1375395

Jurkat-Rott, K., N. Mitrovic, C. Hang, A. Kouzmekine, P. Iaizzo, J. Herzog, H. Lerche, S. Nicole, J. Vale-Santos, D. Chauveau, et al. 2000. Voltage-sensor sodium channel mutations cause hypokalemic periodic paralysis type 2 by enhanced inactivation and reduced current. *Proc. Natl. Acad. Sci. USA.* 97:9549–9554. doi:10.1073/pnas.97.17.9549

Kuzmenkin, A., V. Muncan, K. Jurkat-Rott, C. Hang, H. Lerche, F. Lehmann-Horn, and N. Mitrovic. 2002. Enhanced inactivation and pH sensitivity of Na^+ channel mutations causing hypokalaemic periodic paralysis type II. *Brain.* 125:835–843. doi:10.1093/brain/awf071

Lansman, J.B. 1990. Blockade of current through single calcium channels by trivalent lanthanide cations. Effect of ionic radius on the rates of ion entry and exit. *J. Gen. Physiol.* 95:679–696. doi:10.1085/jgp.95.4.679

Lawrence, J.H., D.W. Orias, J.R. Balser, H.B. Nuss, G.F. Tomaselli, B. O'Rourke, and E. Marban. 1996. Single-channel analysis of inactivation-defective rat skeletal muscle sodium channels containing the F1304Q mutation. *Biophys. J.* 71:1285–1294. doi:10.1016/S0006-3495(96)79329-3

Leffler, A., R.M. Linte, C. Nau, P. Reeh, and A. Babes. 2007. A high-threshold heat-activated channel in cultured rat dorsal root ganglion neurons resembles TRPV2 and is blocked by gadolinium. *Eur. J. Neurosci.* 26:12–22. doi:10.1111/j.1460-9568.2007.05643.x

McPhee, J.C., D.S. Ragsdale, T. Scheuer, and W.A. Catterall. 1995. A critical role for transmembrane segment IVS6 of the sodium channel alpha subunit in fast inactivation. *J. Biol. Chem.* 270:12025–12034. doi:10.1074/jbc.270.20.12025

Papazian, D.M., X.M. Shao, S.A. Seoh, A.F. Mock, Y. Huang, and D.H. Wainstock. 1995. Electrostatic interactions of S4 voltage sensor in Shaker K^+ channel. *Neuron.* 14:1293–1301. doi:10.1016/0896-6273(95)90276-7

Powis, D.A., C.L. Clark, and K.J. O'Brien. 1994. Lanthanum can be transported by the sodium-calcium exchange pathway and directly triggers catecholamine release from bovine chromaffin cells. *Cell Calcium.* 16:377–390. doi:10.1016/0143-4160(94)90031-0

Sheets, M.F., and D.A. Hanck. 1992. Mechanisms of extracellular divalent and trivalent cation block of the sodium current in canine cardiac Purkinje cells. *J. Physiol.* 454:299–320.

Sokolov, S., T. Scheuer, and W.A. Catterall. 2005. Ion permeation through a voltage- sensitive gating pore in brain sodium channels having voltage sensor mutations. *Neuron.* 47:183–189. doi:10.1016/j.neuron.2005.06.012

Sokolov, S., T. Scheuer, and W.A. Catterall. 2007. Gating pore current in an inherited ion channelopathy. *Nature.* 446:76–78. doi:10.1038/nature05598

Sokolov, S., T. Scheuer, and W.A. Catterall. 2008. Depolarization-activated gating pore current conducted by mutant sodium channels in potassium-sensitive normokalemic periodic paralysis. *Proc. Natl. Acad. Sci. USA.* 105:19980–19985. doi:10.1073/pnas.0810562105

Starace, D.M., and F. Bezanilla. 2004. A proton pore in a potassium channel voltage sensor reveals a focused electric field. *Nature.* 427:548–553. doi:10.1038/nature02270

Stefani, E., and F. Bezanilla. 1998. Cut-open oocyte voltage-clamp technique. *Methods Enzymol.* 293:300–318. doi:10.1016/S0076-6879(98)93020-8

Struyk, A.F., and S.C. Cannon. 2007. A Na^+ channel mutation linked to hypokalemic periodic paralysis exposes a proton-selective gating pore. *J. Gen. Physiol.* 130:11–20. doi:10.1085/jgp.200709755

Struyk, A.F., K.A. Scoggan, D.E. Bulman, and S.C. Cannon. 2000. The human skeletal muscle Na channel mutation R669H associated with hypokalemic periodic paralysis enhances slow inactivation. *J. Neurosci.* 20:8610–8617.

Struyk, A.F., V.S. Markin, D. Francis, and S.C. Cannon. 2008. Gating pore currents in DIIS4 mutations of $Na_V1.4$ associated with periodic paralysis: saturation of ion flux and implications for disease pathogenesis. *J. Gen. Physiol.* 132:447–464. doi:10.1085/jgp.200809967

Tombola, F., M.M. Pathak, and E.Y. Isacoff. 2005. Voltage-sensing arginines in a potassium channel permeate and occlude cation-selective pores. *Neuron.* 45:379–388. doi:10.1016/j.neuron.2004.12.047

Tombola, F., M.M. Pathak, P. Gorostiza, and E.Y. Isacoff. 2007. The twisted ion-permeation pathway of a resting voltage-sensing domain. *Nature.* 445:546–549. doi:10.1038/nature05396

Trimmer, J.S., S.S. Cooperman, S.A. Tomiko, J.Y. Zhou, S.M. Crean, M.B. Boyle, R.G. Kallen, Z.H. Sheng, R.L. Barchi, F.J. Sigworth, et al. 1989. Primary structure and functional expression of a mammalian skeletal muscle sodium channel. *Neuron.* 3:33–49. doi:10.1016/0896-6273(89)90113-X

Venance, S.L., S.C. Cannon, D. Fialho, B. Fontaine, M.G. Hanna, L.J. Ptacek, M. Tristani-Firouzi, R. Tawil, and R.C. Griggs; CINCH investigators. 2006. The primary periodic paralyses: diagnosis, pathogenesis and treatment. *Brain.* 129:8–17. doi:10.1093/brain/awh639

Villalba-Galea, C.A., W. Sandtner, D.M. Starace, and F. Bezanilla. 2008. S4-based voltage sensors have three major conformations. *Proc. Natl. Acad. Sci. USA.* 105:17600–17607. doi:10.1073/pnas.0807387105

Yang, N., A.L. George Jr., and R. Horn. 1996. Molecular basis of charge movement in voltage-gated sodium channels. *Neuron.* 16:113–122. doi:10.1016/S0896-6273(00)80028-8

Yarov-Yarovoy, V., D. Baker, and W.A. Catterall. 2006. Voltage sensor conformations in the open and closed states in ROSETTA structural models of K^+ channels. *Proc. Natl. Acad. Sci. USA.* 103:7292–7297. doi:10.1073/pnas.0602350103

Yu, F.H., R.E. Westenbroek, I. Silos-Santiago, K.A. McCormick, D. Lawson, P. Ge, H. Ferriera, J. Lilly, P.S. DiStefano, W.A. Catterall, et al. 2003. Sodium channel beta4, a new disulfide-linked auxiliary subunit with similarity to beta2. *J. Neurosci.* 23:7577–7585.